

Supporting Information

Amination strategy to boost CO₂ electroreduction current density of M-N/C single-atom catalysts to industrial application level

Zhipeng Chen, Xinxin Zhang, Wei Liu, Mingyang Jiao, Kaiwen Mou, Xiangping Zhang, and Licheng Liu*

Experimental Section

1. Synthesis of catalysts

Synthesis of Ni-N₄/C: In a typical synthesis procedure, Zn(NO₃)₂·6H₂O (4.76 g) and nickel(II) acetylacetonate (Ni(acac)₂, 0.41 g) were dissolved in 60 mL of methanol, which was subsequently added into 60 mL methanol containing 2-methylimidazole (MeIM, 5.26 g) under vigorously stirring for 60 min at room temperature, and then the mix solution was grown under static at room temperature for 24 h. Next, the as-obtained precipitates were centrifuged and washed with methanol three times and dried in vacuum at 60 °C for 12 h. Finally, the as-prepared Ni-doped ZIF-8 was pyrolyzed at 1000 °C for 3 h with a heating rate 5 °C min⁻¹ in a stream (25 sccm) of Ar to yield Ni-N₄/C. During the pyrolysis process, Zn would be evaporated away (melting point of 420 °C, boiling point of 907 °C, only trace amounts of Zn (~0.007 wt%) was detected by ICP-OES.) and Ni ions would be reduced by carbonized organic linkers, leaving atomically dispersed Ni atoms anchored on nitrogen-doped carbon.

Synthesis of Ni-N₄/C-NH₂: In a general procedure, as-prepared Ni-N₄/C (0.10 g) was firstly mechanically mixed with carbamide (5.00 g) by an agitated mortar for 30 min, and then the fine powder mixture was pyrolyzed at 450 °C for 3 h with a heating rate 5 °C min⁻¹ in a stream (15 sccm) of NH₃. Next, the as-obtained catalyst was impregnated with the mixed solution of ammonia (25%) and ethanol (V:V=2:1, 50 mL) and stirred for 24 h. Subsequently, the obtained precipitate was dispersed in ammonia water (35 mL) and then was sealed in a Teflon-lined stainless steel autoclave and heated to 150

°C for 12 h. Finally, the suspension was centrifuged, and then the precipitate was washed with deionized water and dried in vacuum at 60 °C for 24 h to obtain Ni-N₄/C-NH₂ catalyst. As-prepared catalysts were directly used without any post-treatment.

It should be noted that if the catalyst was prepared without the step of pyrolysis with carbamide, the agglomeration of Ni single atoms will occur (Figure S1).

Synthesis of Fe-N/C: Fe-N/C was synthesized by the similar procedure as the Ni-N₄/C, except that iron(III) acetylacetonate (0.56 g) was used instead of nickel(II) acetylacetonate.

Synthesis of Aminated Fe-N/C: Aminated Fe-N/C was synthesized by the similar procedure as Ni-N₄/C-NH₂, except that Fe-N/C was used instead of Ni-N₄/C.

Synthesis of Zn-N/C: Typically, zinc acetate dihydrate (Zn(OAc)₂·2 H₂O, 0.20 g) was firstly mechanically mixed with melamine (C₃H₆N₆, 6.00 g) and L-alanine (C₃H₇NO₂) (1.20 g) by an agitated mortar for 30 min. Next, the fine powder mixture was first pyrolyzed at 600 °C for 2 h with a heating rate 3 °C min⁻¹, and then heated to 900 °C for 1 h at a heating rate 2 °C min⁻¹ in a stream (50 sccm) of Ar. After cooling down to room temperature, the carbonized precursor powder was successively in 3 M H₂SO₄ for 12 h and 3 M HNO₃ for another 12 h under continuous stirring at 80 °C. After centrifugation with deionized water to neutral pH, the catalyst precursor dried in vacuum at 60 °C for overnight. Subsequently, the sample was separately re-pyrolyzed at 900 °C for 1 h with a heating rate 5 °C min⁻¹ in a stream 40 sccm of Ar to enhanced the crystallinity of carbon.

Synthesis of Aminated Zn-N/C: Aminated Zn-N/C was synthesized by the similar procedure as Ni-N₄/C-NH₂, except that Zn-N/C was used instead of Ni-N₄/C.

It should be clear that all the catalysts were independently synthesized and analyzed at least three times in this work.

2. Preparation of working electrodes.

The substrate electrode using in H-type cell was fabricated by carbon cloth (1×1 cm), which was sonicated in hydrochloric acid (10 M), acetone, and deionized water for 30 min, respectively. Typically, powder catalysts (12.0 mg) were dispersed in Nafion perfluorinated resin solution (5 wt%, 120 μL) and isopropanol (600 μL) by ultrasonication for 30 min to form homogeneous catalysts ink. Then the as-prepared catalyst ink was sprayed onto the carbon cloth several times with a 20 μL pipette, using 360 μL for each electrode. Finally, the obtained composite electrodes were dried at 50 °C for 12 h, and the catalyst loading is $3.0 \pm 0.1 \text{ mg cm}^{-1}$.

Carbon paper (Freudenberg H14C9) with a Micro Porous layer (MPL) and hydrophobic treatment (PTFE) was used as gas diffusion layer (GDL). Powder catalyst was coated on the MPL face of GDL by the same method as the carbon cloth electrode using in H-type cell, and the catalyst-supported GDL was used as GDE in flow cell.

3. Electrochemical experiments in H-type cell

Electrochemical experiments were performed in a gas-tight H-cell containing 25 mL of electrolyte, which was separated by a proton exchange membrane (Nafion N117). Ag/AgCl (saturated KCl) electrode and Pt plate (1×1 cm) were used as reference and counter electrodes, respectively. Electrochemical data were recorded on a CHI660E electrochemical workstation. Before each experiment, CO₂ (99.999%) was continuously bubbled into electrolyte for 30 minutes to eliminate O₂, and saturate electrolyte with CO₂. Electrochemical experiments were measured at room temperature (25±3 °C), and all potentials reported in this paper are referenced to reversible hydrogen electrode (RHE, $E_{\text{RHE}} = E_{\text{Ag/AgCl}} + 0.197 + 0.0591 \times \text{pH}$), and an automatic iR compensation (85%) was used. The pH of N₂ and CO₂-saturated 0.5 M KHCO₃ electrolyte in this study is 8.56 and 7.33, respectively. Linear sweep voltammetry (LSV) was carried out in CO₂-saturated or N₂-saturated 0.5 M KHCO₃ electrolyte with a scan rate of 50 mV s⁻¹. Electrochemical impedance spectroscopy (EIS) was recorded at -1.0 V in CO₂-saturated 0.5 M KHCO₃ electrolyte with an amplitude of 5 mV, and the frequency range is from 0.1 Hz to 10000 Hz. Tafel plot (overpotential versus $\log j_{\text{HCOO}^-}$) was derived

from the controlled potential electrolysis results. Electrocatalytic reduction of CO₂ was investigated for 30 min at each applied potential by controlled potential electrolysis method. Prior to each new electrolysis, 50 cycles of cyclic voltammetry (CV) were used to activate the catalysts. Stirring (1000 rpm) was applied during CO₂ electrocatalytic reduction.

4. Electrochemical experiments in flow cell

Electrochemical experiments in flow cell was performed in a four-part self-made microflow cell (Figure 3a) using constant potential electrolysis method, and an automatic iR compensation was used. Catalyst-supported GDE, Ag/AgCl (saturated KCl) electrode equipped with a salt bridge, and squashed nickel foam (0.2 mm thickness, 400 mesh) were used as cathode (for CO₂ reduction), reference electrode and anode (for O₂ evolution), respectively. Cathode and anode are respectively connected with copper tape (current collector). Three chambers of catholyte, anolyte and CO₂ gas diffusion were made of polytetrafluoroethylene (PTFE), and the depth of each chamber is 0.3 cm. Each chamber had an inlet and an outlet for electrolyte or CO₂ gas, and reference electrode was fixed in catholyte chamber. Cathode were placed between CO₂ gas diffusion chamber and electrolyte chamber, and an anionic exchange membrane (Fumasep FAB-PK-130) was interposed between anolyte and catholyte chamber. Cathode area was controlled to 1 cm² (2.0×0.5 cm) when assembling the cell, and a silicone gasket was placed between each GDE, anionic exchange membrane and electrolyte chamber for sealing. 300 mL of catholyte (1 M KOH) was circulated in cathode chamber by means of a peristaltic pump at a constant flow 35 mL min⁻¹. It should be emphasized that anolyte (1 M KOH) was circulated through anode chamber by using a specially-made gas-liquid mixed flow pump instead of conventional peristaltic pump, which can effectively remove O₂ produced in anode chamber in time, and this is one of key conditions for obtaining ultra-high current density in this flow cell configuration. High purity CO₂ was purged in the back chamber of catholyte chamber at a constant flow 30 sccm by mean of a digital mass flow controller, and CO₂ output was connected to a GC system.

It must be explained here, the catalytic activity datas of CO₂RR in both H-type cell and flow cell are the mean values obtained from three independent experiments, thus the error bars are just the standard deviations (Mean±S.D.) in this manuscript.

5. Computational Details

Density function theory calculation were performed by using the CP2K package.^[1] Perdew-Burke-Ernzerhof (PBE) functional with Grimme D3 correction was used to describe the nonlocal exchange and correlation energies.^[2, 3] Since the generalized gradient functional fails to reproduce the correlated elements, we adopted the “+U” Hubbard correction for the 3d electrons.^[4] It's known that quantitatively results depends on the choice of U value. The U value of 3.4 eV has been used for Ni metal center, which provides a satisfying overall description of electronic structure and surface reactivity for single atom catalyst.^[5] Unrestricted Kohn-Sham DFT has been used as the electronic structure method in the framework of the Gaussian and plane waves method.^[6, 7] The norm-conserving Goedecker-Teter-Hutter (GTH) pseudopotentials, DZVP-MOLOPT-GTH basis sets were utilized to describe core electrons of all elements.^[8-10] Gaussian function with molecularly optimized double-zeta polarized basis sets (m-DZVP) were used for describing the wave function of Ni 3d⁸4s², C 2s²2p², N 2s²2p³ and H 1s¹ electrons. A plane-wave energy cut-off of 500 Ry has been employe. During the calculations, all the atomic positions were fully relaxed until the force is smaller than 0.05 eV/Å. All models were applied with a 20 Å vacuum layer.

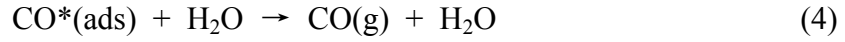
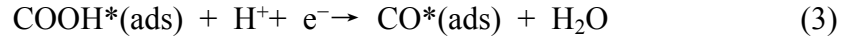
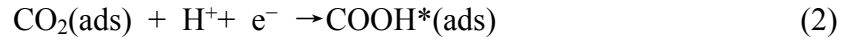
The potential-dependence of reaction free energies in elementary steps involving proton-electron transfers was evaluated using the computational hydrogen electrode (CHE) approach.^[11] For every proton-electron transfer step, the potential-dependent chemical potential of a proton electron pair was used to determine the relative free energy.

In this approach, a reversible hydrogen electrode (RHE) is used as a reference:



where the proton-electron pairs are in equilibrium with H₂ at all values of pH and 1 atm of H₂, without potential bias.

Reaction mechanism for electrocatalytic reduction of CO₂ to CO(g) is suggested as follows:



CO₂ molecule adsorbed on catalyst surface first receive an electron from catalyst and couple a H⁺ to form formate intermediate COOH*, and then COOH* continued to obtain an electron and a H⁺ to generate adsorbed CO*(ads) and H₂O. Finally, CO*(ads) desorb from the surface of catalyst to form CO(g).

The Gibbs free energy is calculated using:

$$\Delta G_{\text{free}} = \Delta E_{\text{DFT}} + \Delta E_{\text{ZPE}} - T\Delta S \quad (5)$$

Where ΔG_{free} is gibbs free energy, E_{DFT} is electronic energy calculate from DFT, S is entropy, T is temperature (300 K), and E_{ZPE} is zero point energy estimated at the harmonic approximation by calculating vibrational frequency of the adsorbate or molecule.

Charge density difference is defined as:

$$\Delta\rho = \rho_{\text{mol/sur}} - \rho_{\text{mol}} - \rho_{\text{sur}} \quad (6)$$

Where $\rho_{\text{mol/sur}}$, ρ_{mol} , and ρ_{sur} are the electron density of molecule adsorbed on surface, and individual electron density of molecule and surface.

Adsorption energy (E_{ads}) (binding energy) is defined as:

$$E_{\text{ads}} = E_{\text{mol/sur}} - E_{\text{mol}} - E_{\text{sur}} \quad (7)$$

Where $E_{\text{mol/sur}}$, E_{mol} and E_{sur} are the energies of molecule adsorbed on surface, and individual electron density of molecule and surface.

6. Characterization and Products Analysis

X-ray absorption fine structure spectra (XAFS) was collected at BL14W1 beamline of Beijing Synchrotron Radiation Facility (BSRF) with a fluorescence model, and Ni foil, NiO, and Ni^(II)PC were used as standard reference samples.

Transmission electron microscopy (TEM) was performed on a Tecnai G2 20 transmission electron microscope operated at 200 kV accelerating voltage. High resolution TEM (HRTEM) and high-angle annular dark-field scanning transmission electron microscopy (HAADF-STEM) images and elemental mappings were collected by a JEOL ARM-200F field-emission transmission electron microscope. Fourier transform (FT)-IR spectra were performed on the FT-IR spectrometer (Nexus 470) with a KBr disk containing catalysts powder. X-ray diffraction (XRD) patterns were recorded on a Bruker D2 Phaser X-Ray powder Diffractometer with (Cu K α radiation, $\lambda = 0.15406$ nm). X-ray photoelectron spectroscopy (XPS) was recorded on a PHI Quantera SXM spectrometer. All the binding energy corresponds to the standard C1s peak at 284.8 eV in this experiment. Inductively Coupled Plasma Optical Emission Spectrometry (ICP-OES) was carried on an Atomscan Advantage (Thermo Jarrell Ash, USA). CO₂ adsorption isotherms were determined by a Micromeritics ASAP 2020M at 25 °C, and before CO₂ adsorption experiment, two cycles of gas desorption were performed.

The concentration of gaseous samples (CO and H₂) was measured by on-line gas chromatography (GC, Inficon S3 Micro 3000 GC), which was equipped with flame ionization detector (FID) and thermal conductivity detector (TCD). Gas products were directly connected to GC for on-line analysis during the electrolysis reaction. H₂ and CO concentration was analyzed by the TCD and FID detectors, respectively. Liquid phase products were quantified by a high performance liquid chromatography (HPLC, Hitachi Primaide 1020) with the Bio-Rad Aminex HPX-87H column, and a 0.5 M H₂SO₄ was used as the mobile phase.

Faradaic efficiency (η) of CO and H₂ was calculated by the formula:

$$\eta = 2nF / Q$$

where η is Faradaic efficiency of products; 2 represents the number of electrons required to form CO and H₂ from CO₂; n represents the total number of moles of CO and H₂ production, which was measured by GC; F represents Faraday constant (96485); and the Q corresponds to the amount of cumulative charge in the process of CO₂ reduction, which was provided by the electrochemical workstation.

Supplementary Figures

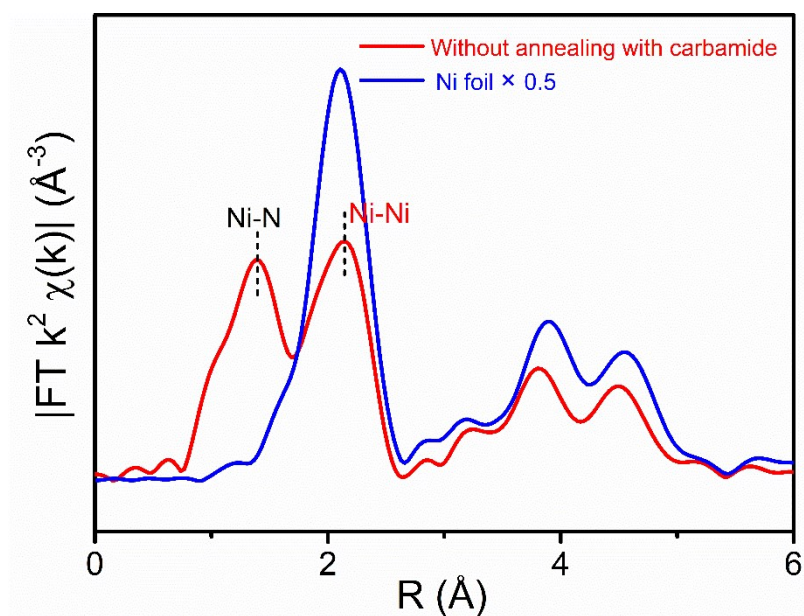


Figure S1. Fourier transformation of EXAFS spectra for Ni K-edge of Ni foil and $\text{NiN}_4/\text{C-NH}_2$ prepared without the step of annealing with carbamide. The Ni-Ni path at 2.09 \AA indicates the occurrence of Ni agglomeration.

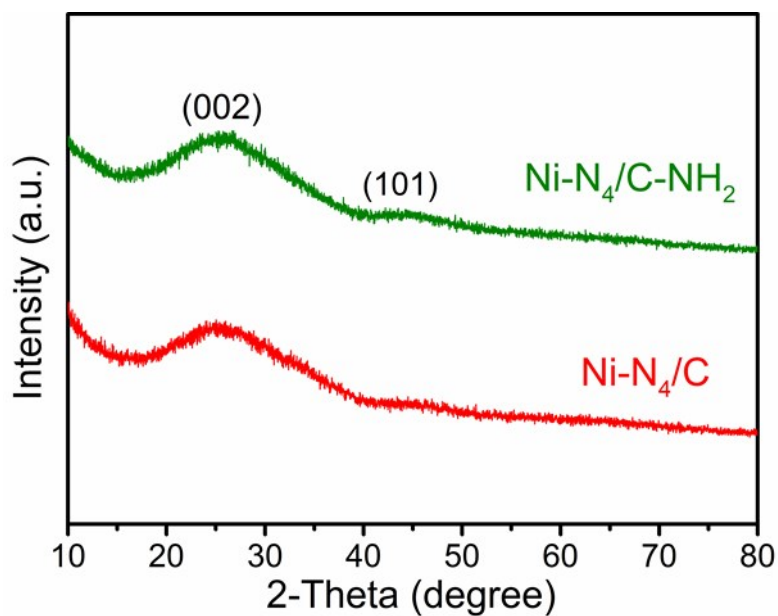


Figure S2. XRD patterns of $\text{Ni-N}_4/\text{C}$ and $\text{Ni-N}_4/\text{C-NH}_2$. The two broad diffraction peaks centered at 26° and 44° are assigned to (002) and (100) planes of graphite carbon.

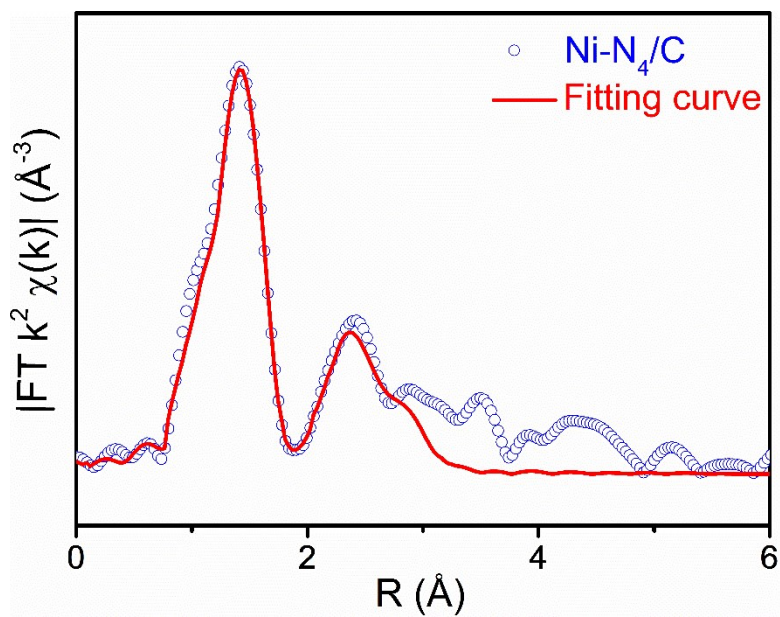


Figure S3. Fitting for EXAFS spectrum of Ni-N₄/C.

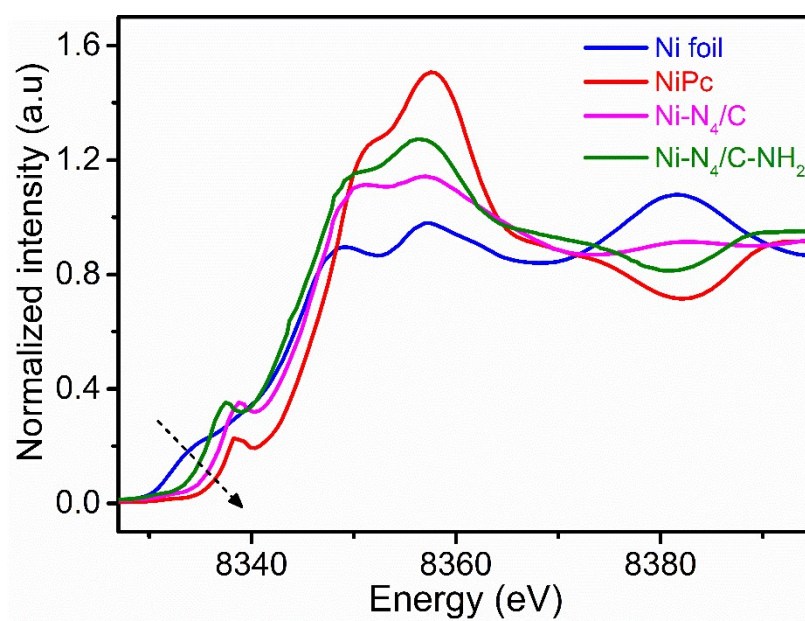


Figure S4. XANES spectra at the Ni K-edge of Ni foil, NiPc, Ni-N₄/C, and Ni-N₄/C-NH₂.

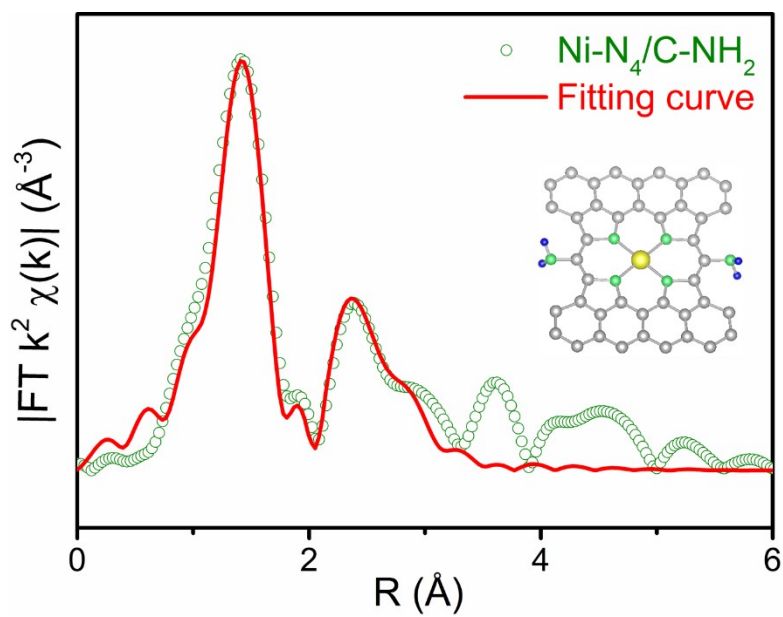


Figure S5. Fitting for EXAFS spectrum of Ni-N₄/C-NH₂, inset is Ni-N₄/C-NH₂ structure.

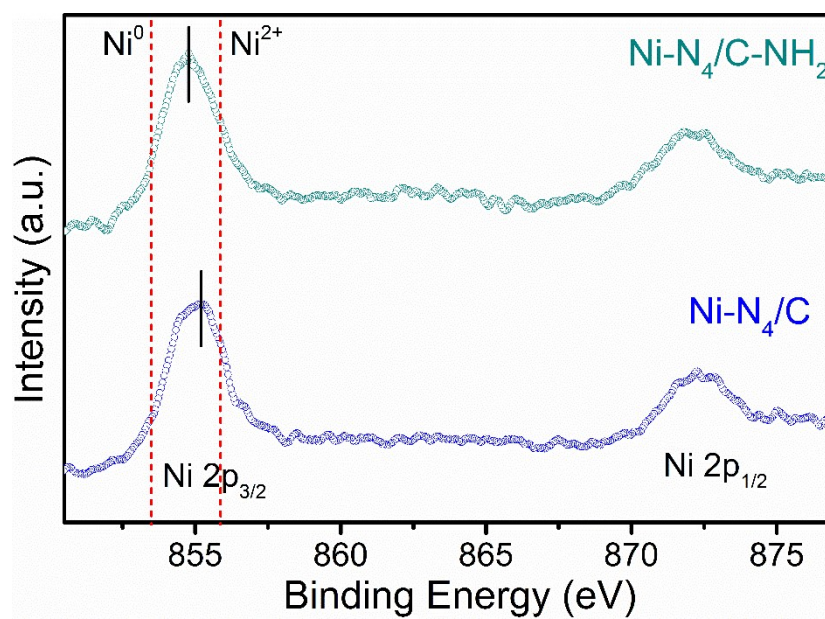


Figure S6. Ni 2p XPS spectra of Ni-N₄/C-NH₂ and Ni-N₄/C.

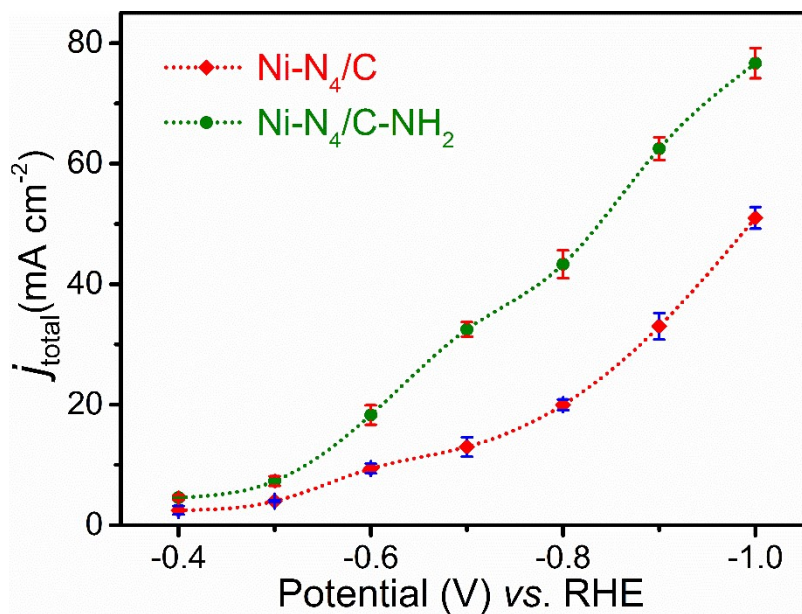


Figure S7. Total current density of Ni-N₄/C-NH₂ and Ni-N₄/C at different electrolytic potentials in H-type cell.

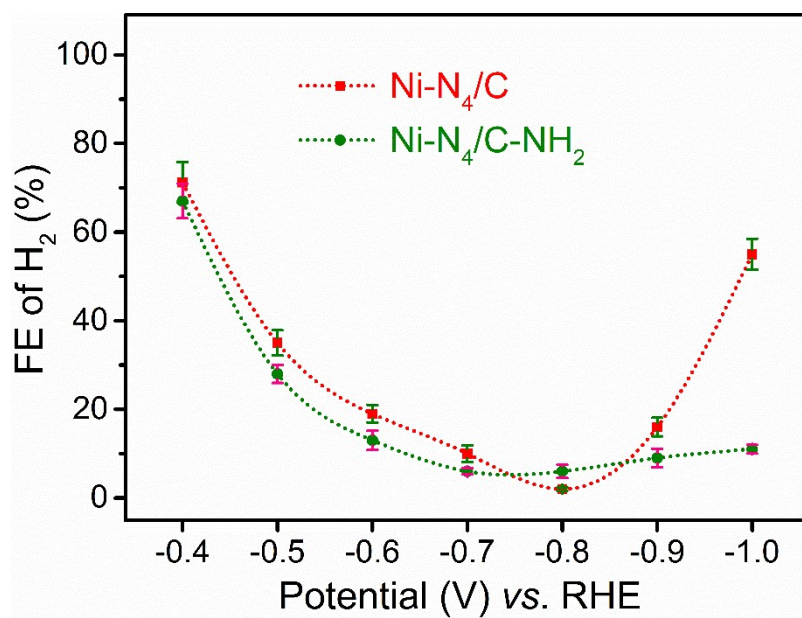


Figure S8. FE of H₂ production of Ni-N₄/C-NH₂ and Ni-N₄/C in H-type cell.

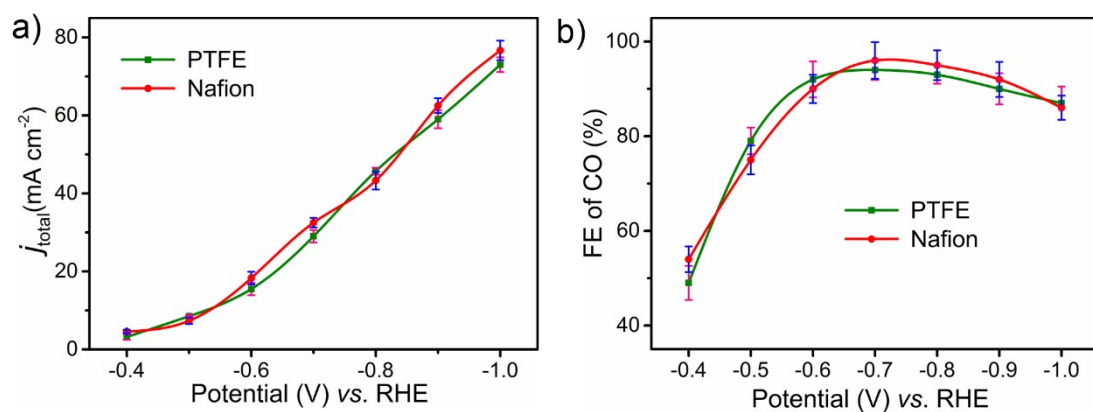


Figure S9. Electrocatalytic activity tests of Ni-N₄/C-NH₂ catalysts prepared with different ionomer binder in H-type cell. a) Total current density and b) CO FE.

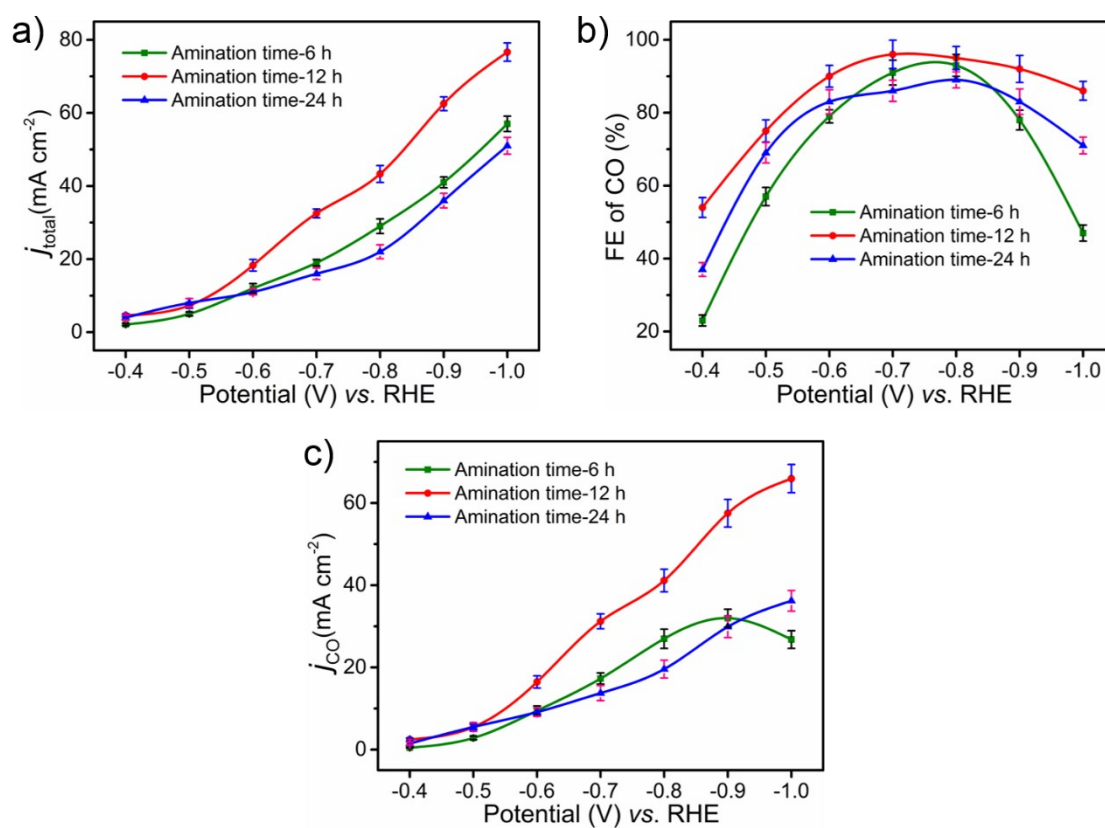


Figure S10. Electrocatalytic activity tests of Ni-N₄/C-NH₂ catalysts under different amination time in H-type cell. a) Total current density, b) CO FE, and c) CO partial current density.

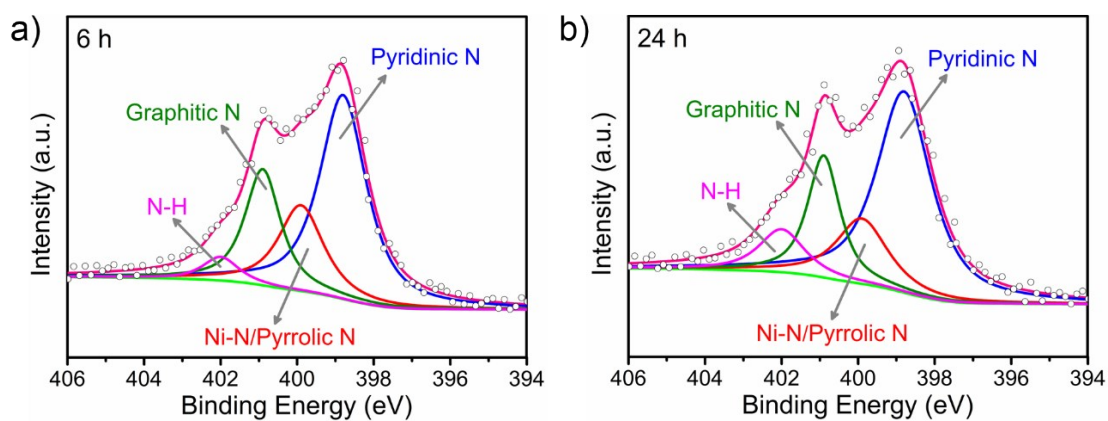


Figure S11. N 1s XPS spectra of Ni-N₄/C-NH₂ prepared at different amination time, (a) 6 h and (b) 24 h.

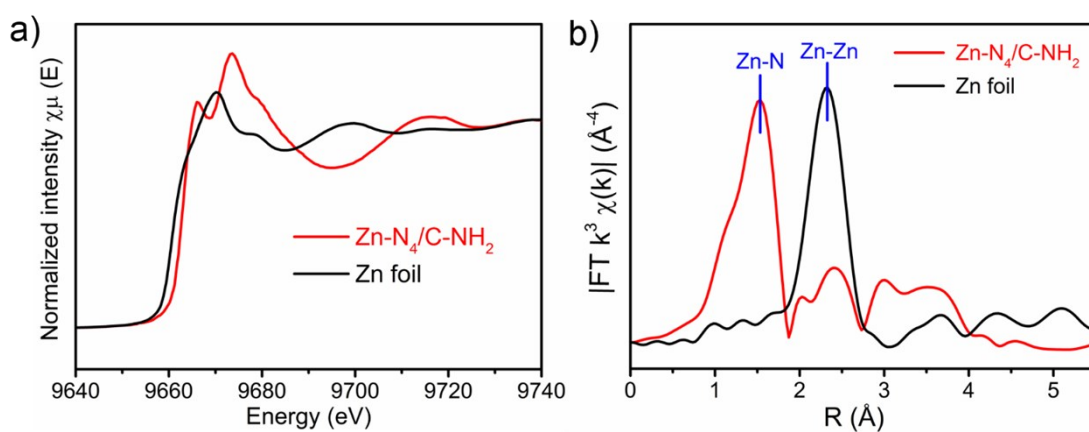


Figure S12. a) XANES spectra, b) Fourier transformation of EXAFS spectra at the Zn K-edge of Zn foil and Zn-N₄/C-NH₂.

The XAFS results demonstrate the single atomic dispersion of Zn atoms, and no agglomerated Zn particles were observed.

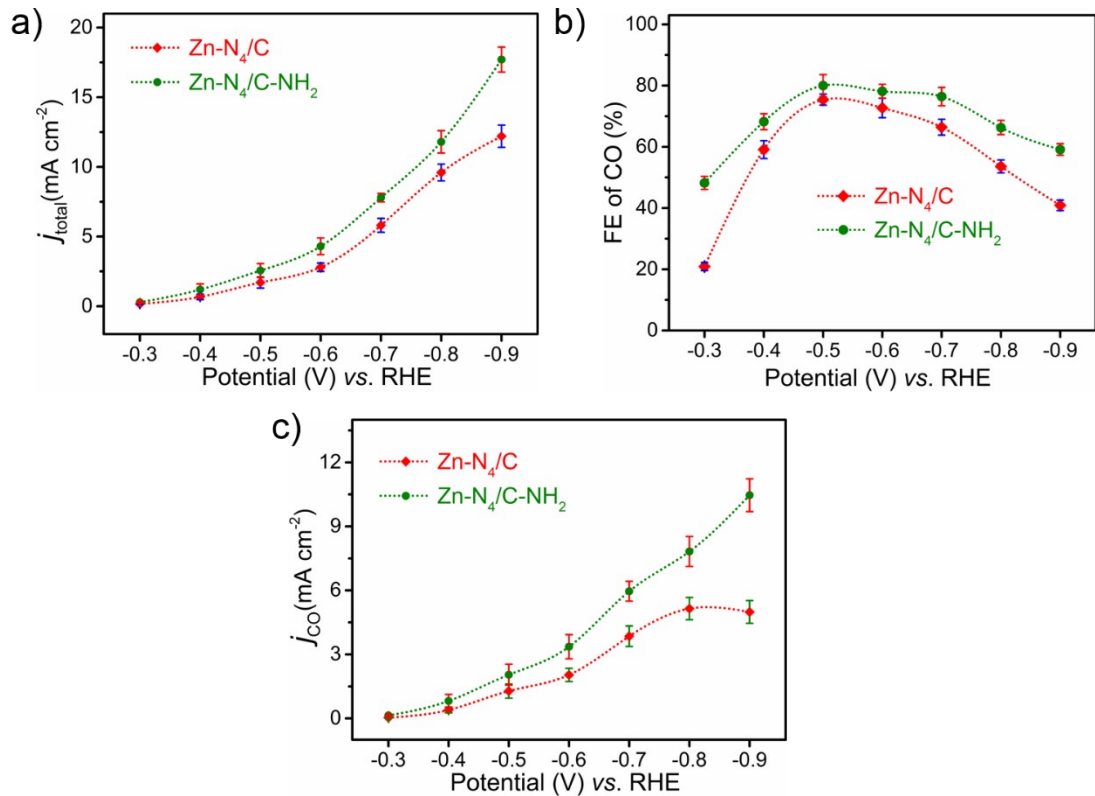


Figure S13. Electrocatalytic activity tests in H-type cell. a) Total current density, b) CO FE, and c) CO partial current density of Zn-N₄/C and Zn-N₄/C-NH₂. After amino-modification, the Zn-N₄/C-NH₂ exhibits a larger CO FE, and CO partial current density has increased by 2.1 times.

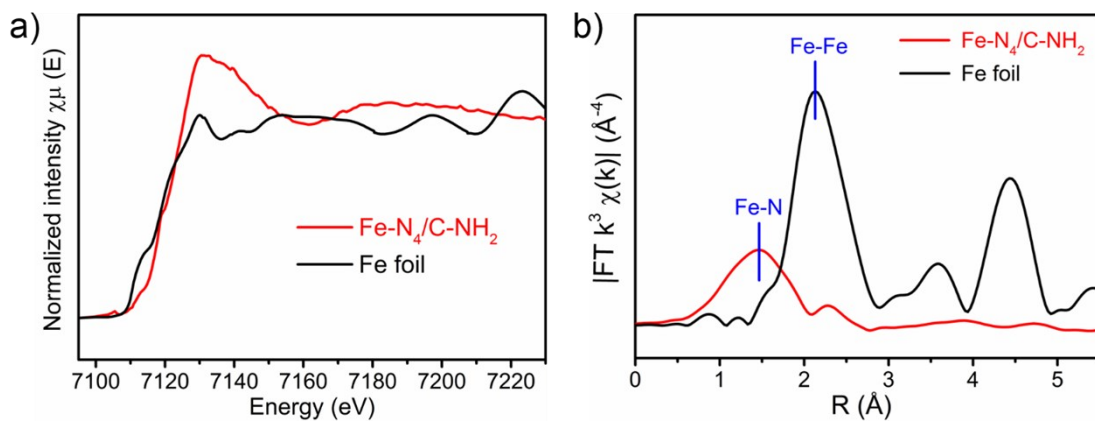


Figure S14. a) XANES spectra, b) Fourier transformation of EXAFS spectra at the Fe K-edge of Fe foil and Fe-N₄/C-NH₂.

The XAFS results demonstrate the single atomic dispersion of Fe atoms, and no agglomerated Fe particles were observed.

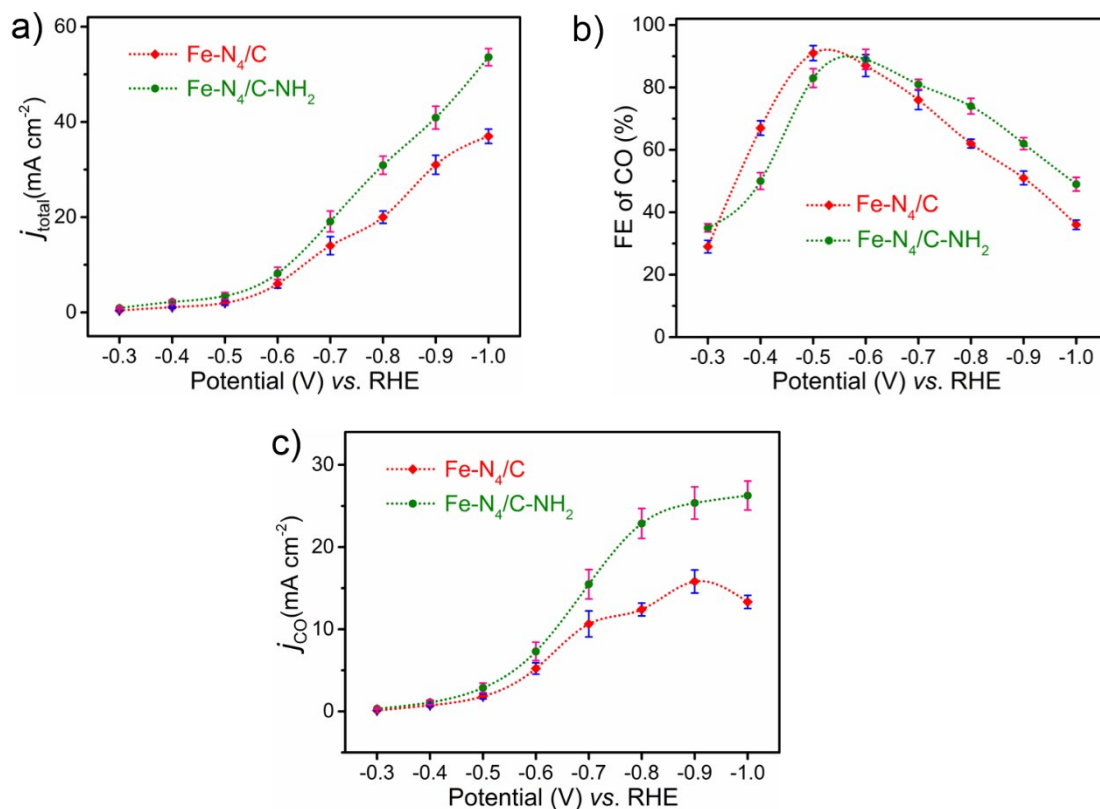


Figure S15. Electrocatalytic activity tests in H-type cell. a) Total current density, b) CO FE, and c) CO partial current density of Fe-N₄/C and Fe-N₄/C-NH₂. After amino-modification, the Fe-N₄/C-NH₂ exhibits an enhanced current density and CO FE, and CO partial current density has increased by 1.7 times.

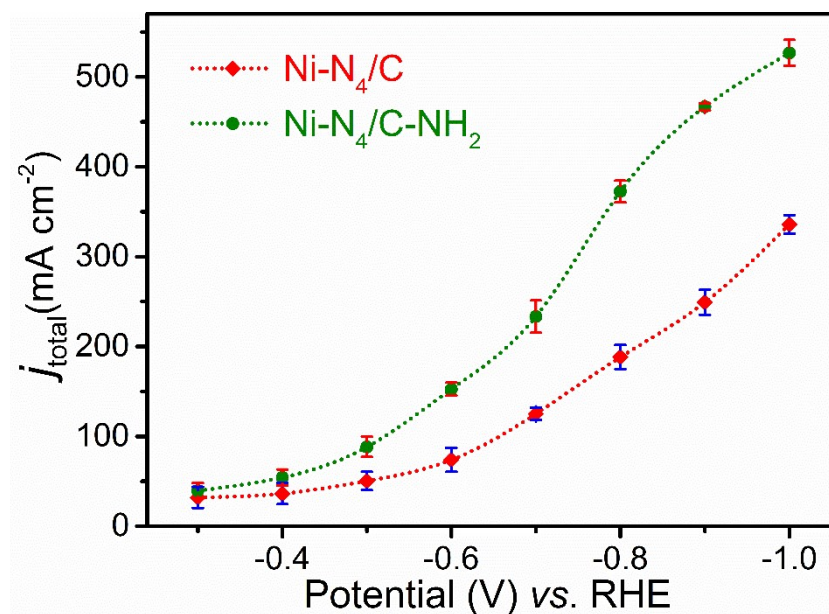


Figure S16. Total current density of Ni-N₄/C and Ni-N₄/C-NH₂ in flow cell.

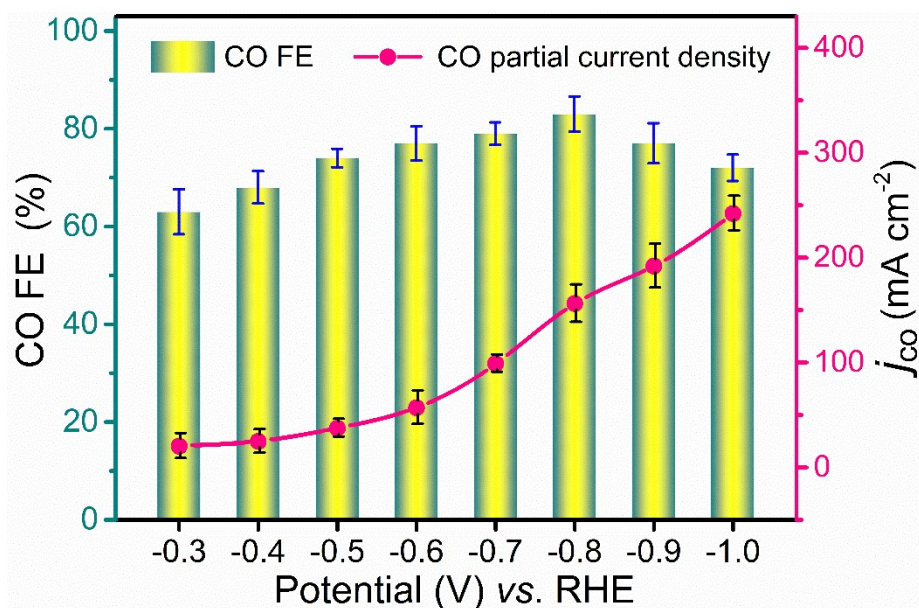


Figure S17. CO FE and CO partial current density of Ni-N₄/C in flow cell.

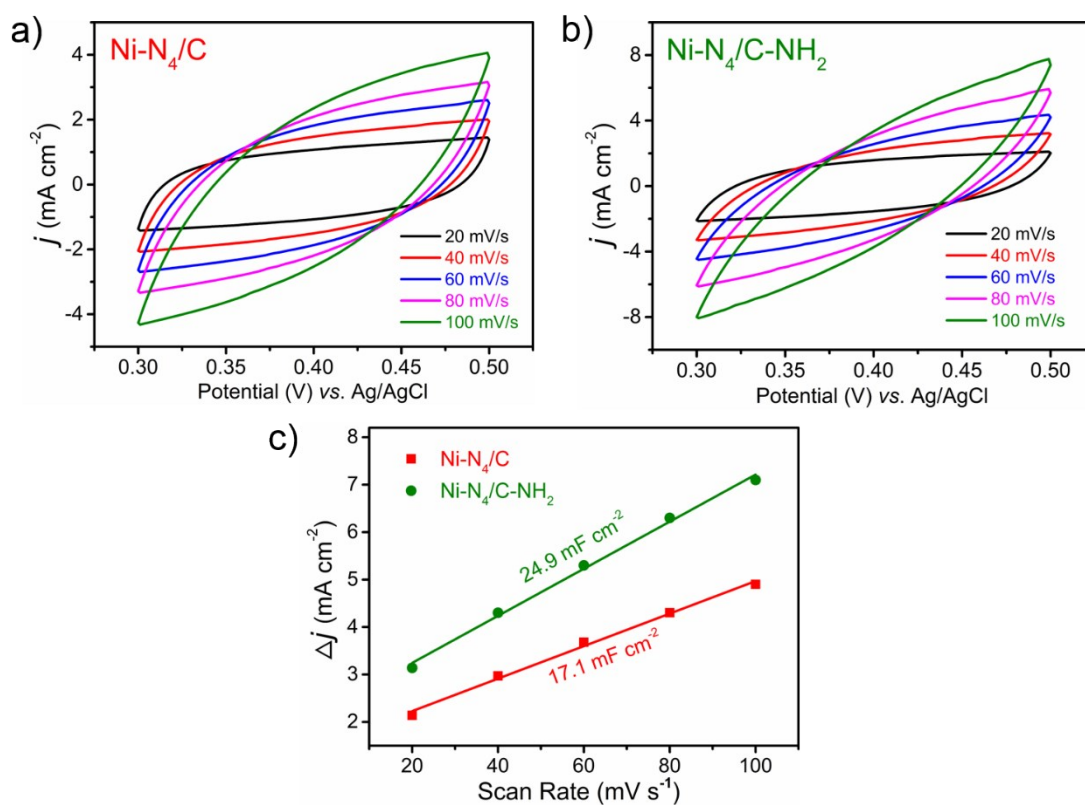


Figure S18. Cyclic voltammograms at the range of 0.30 to 0.50 V vs. Ag/AgCl (sat. KCl) with different scan rates (20, 40, 60, 80, and 100 mV·s⁻¹) for Ni-N₄/C (a), and Ni-N₄/C-NH₂ (b) in H-type cell. Linear fitting of double-layer capacitive currents Δj ($j_a - j_c$) at 0.40 V vs. scan rates to estimate ECSA (c).

The ECSA of catalysts is estimated from the electrochemical double-layer capacitance (Cdl), which is derived from the cyclic voltammograms at a non-Faradaic potential range. The slope of the fitted lines represents the twice Cdl.

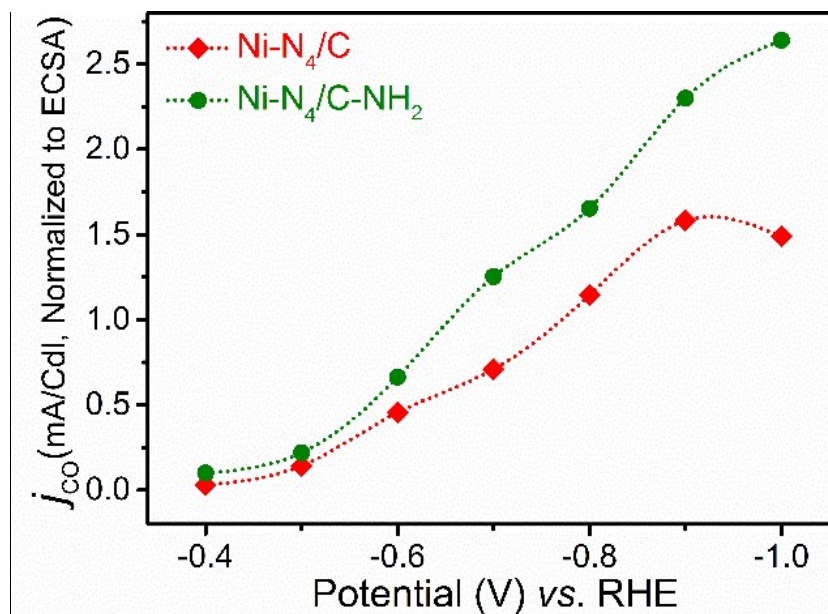


Figure S19. CO partial current density normalized to ECSA of Ni-N₄/C-NH₂ and Ni-N₄/C in H-type cell.

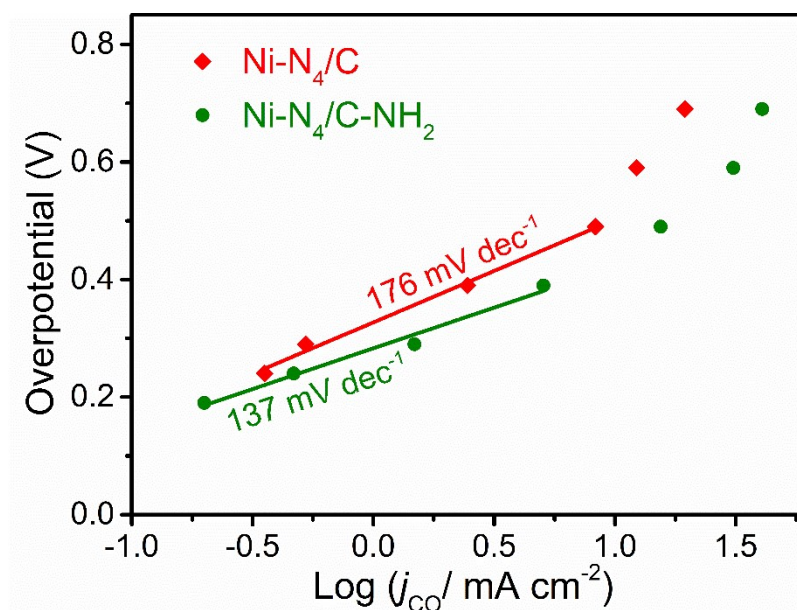


Figure S20. Tafel plots of Ni-N₄/C-NH₂ and Ni-N₄/C in H-type cell.

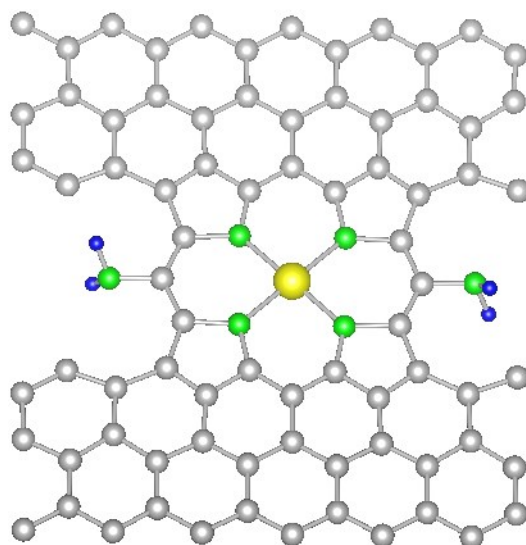


Figure S21. Atomistic structure of Ni-N₄/C-NH₂ viewed in extended simulation cells.

Ni: yellow, N: green, C: gray, H: blue

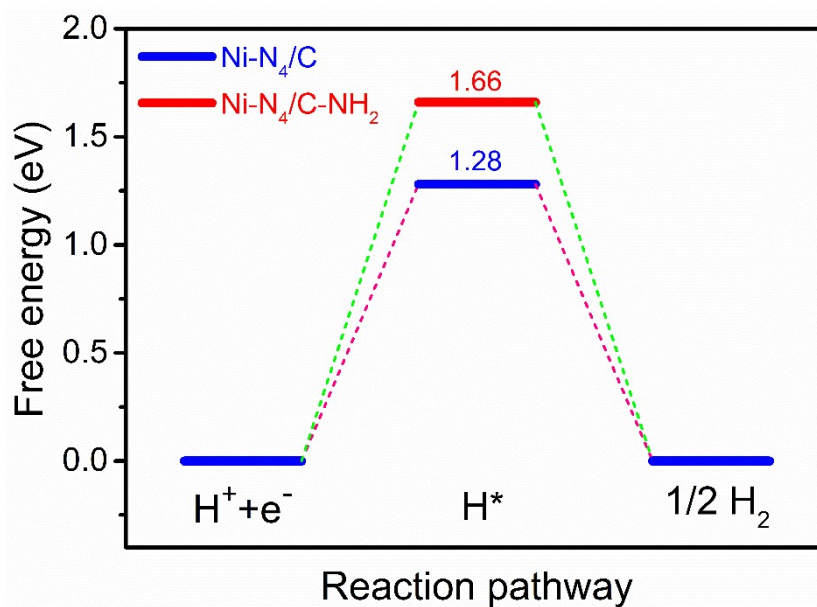


Figure S22. Calculated free-energy diagram of HER over Ni-N₄/C-NH₂ and Ni-N₄/C.

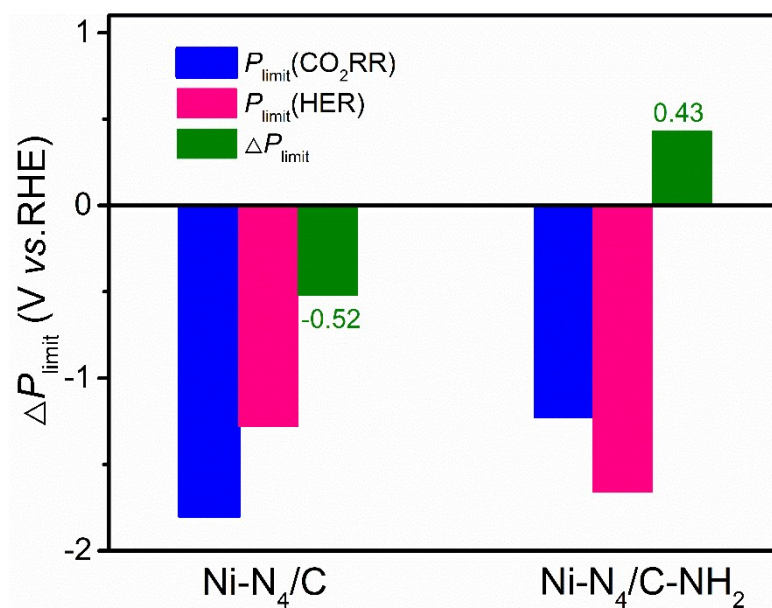


Figure S23. Calculated limiting potentials for CO₂RR and HER of Ni-N₄/C-NH₂ and Ni-N₄/C. ΔP_{limit} is directly related to the selectivity to CO, and a more positive ΔP_{limit} means a higher CO selectivity.

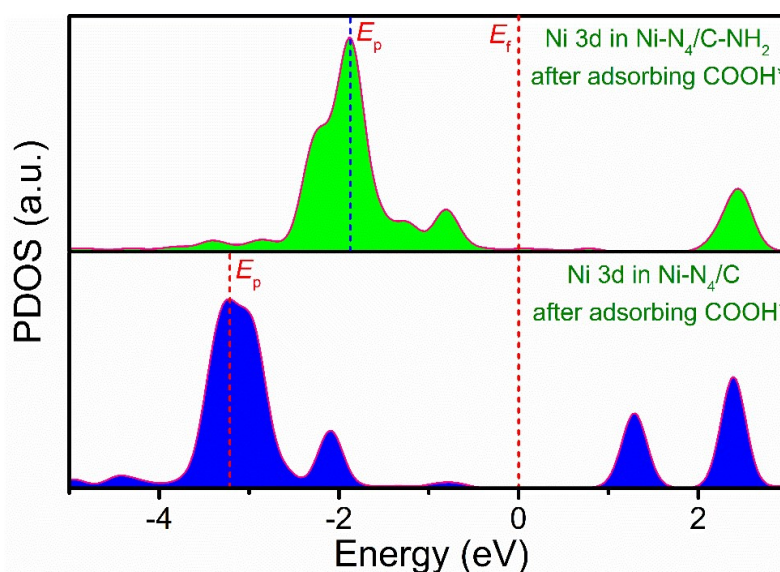


Figure S24. Calculated Ni 3d projected DOS of Ni-N₄/C-NH₂ and Ni-N₄/C after adsorbing COOH*, respectively, E_f is at 0 eV. The adsorption strength of intermediates can be inferred from position of the highest pelectronic states (E_p). The energy level

position of the E_p closer to the Fermi level (E_f) means the lower filling of anti-bonding states, corresponding to the stronger bonding to the adsorbate.

Supplementary Tables

Table S1. Structural parameters obtained from the XAFS fitting

Sample	Bond type	CN	R(Å)	$\sigma^2 \times 10^3$	R-factor
Ni-N ₄ /C-NH ₂	Ni-N	3.83	1.89±0.01	1.8±0.5	0.021
Ni-N ₄ /C	Ni-N	3.79	1.89±0.01	1.3±0.8	0.015

CN, coordination number; R, distance between absorber and backscatter atoms; σ^2 , Debye-Waller factor.

Table S2. The percentage of different configuration of nitrogen

Aminated time	Pyridinic N (%)	Ni-N/Pyrrolic N (%)	Graphitic N (%)	N-H (%)
6 h	52.2	21.2	22.3	4.5
12 h	53.6	20.0	18.5	7.9
24 h	54.4	16.7	19.4	9.5

Table S3. Comparison of the electrocatalytic performance of our catalysts with other state-of-the-art single-atom catalysts reported recently for CO₂RR

Catalysts	Potentials (V)	CO FE (%)	CO partial current density (mA cm ⁻²)	Referencs
This work Flow cell	-1.0	85	447.6	—
	-0.8	89	327.8	—
This work H-type cell	-1.0	87	63.6	—
	-0.8	95	41.2	—
NiSA/PCFM	-1.0	88	308.4	(2020) <i>Nat. Commun</i> ^[12]
Ni-NCB	—	99%	>100	(2019) <i>Joule</i> ^[13]
Ni-N-C	-1.0	85%	~200	(2019) <i>Energy. Environ. Sci</i> ^[14]
Fe ³⁺ -N-C	-0.45	90	94	(2019) <i>Science</i> ^[15]

A-Ni-NSG	-1.0	93	107	(2018) <i>Nat. Energy</i> [16]
CoPc	—	95	150	(2019) <i>Science</i> [17]
NiN-GS	-0.82	93.2	20	(2019) <i>Chem</i> [18]
Bi SAs/NC	-0.5 V	97	3.9	(2019) <i>JACS</i> [19]
NiSA-N-CNTs	-0.7	91.3	23.5	(2018) <i>Adv. Mater</i> [20]
ZnN _x /C	-0.43	95	4.8	(2018) <i>Angew</i> [21]
SAs-Ni-N-C	-0.7	98.5	4	(2020) <i>Nano-Micro Letters</i> [22]
Ni SAs/N-C	-1.00	71.9	10.5	(2017) <i>JACS</i> [23]
SE-Ni SAs@PNC	-1.0	88	18.3	(2018) <i>Angew</i> [24]
Ni-NG	-0.62	95	11	(2018) <i>Energy. Environ. Sci</i> [25]
Ni SAs/NCNTs	-0.75	95	20	(2019) <i>Appl. Catal.-B:Environ.</i> [26]
Ni-N-C	-0.78	85	9.5	(2017) <i>Nat. Commun</i> [27]
Fe-N ₄ -C ₁₀	-0.58	93	2.8	(2018) <i>ACS Catal.</i> [28]
Co-N ₂ -C	-0.52	94	18.1	(2018) <i>Angew</i> [29]
C-AFC@ZIF-8	-0.63	93	10	(2017) <i>Nano Energy</i> [30]
Co-N ₅ -C	-0.79	99	10.2	(2017) <i>JACS</i> [31]
Ni-N ₄ -C	-0.81	28.6	99	(2017) <i>JACS</i> [32]
H-CPs	-1.0	97	48.7	(2019) <i>Joule</i> [33]
D-Sn/N-C1000	-0.8	91	5.1	(2018) <i>Adv. Energy Mater.</i> [34]
Co-Tpy-C	-1.1	93	14.9	(2020) <i>Small</i> [35]
Fe _{0.5d} -N-C	-0.5	80	4.5	(2017) <i>ACS Catal.</i> [36]
Ni-N-MEGO	-0.7	92.1	26.8	(2019) <i>Appl. Catal.-B:Environ.</i> [37]
Fe/NG-750	-0.57	80	1.7	(2018) <i>Adv. Energy Mater.</i> [38]

Axial Fe-N/CN	-1.0	50	~10	(2020) <i>Appl. Catal.-B: Environ.</i> [39]
---------------	------	----	-----	---

Table S4. The fitting values of EIS equivalent circuit

Electrocatalysts	R_s/Ω	R_{ct}/Ω
Ni-N ₄ /C (H-type cell)	6.9	29.6
Ni-N ₄ /C-NH ₂ (H-type cell)	6.3	15.2
Ni-N ₄ /C-NH ₂ (Flow cell)	2.0	7.7

R_s includes bulk resistance of electrodes and contact resistance between electrodes and electrolyte. R_{ct} indicates interfacial charge transfer resistance during electrochemical reactions.

References

- [1] A. A. Peterson, F. Abild-Pedersen, F. Studt, J. Rossmeisl, J. K. Nørskov, *Energy Environ. Sci.* **2010**, 3, 1311.
- [2] G. Stefan, *J. Comput. Chem.* **2010**, 27, 1787.
- [3] J. P. Perdew, K. Burke, M. Ernzerhof, *Phys. Rev. Lett.* **1996**, 77, 3865.
- [4] S. L. Dudarev, G. A. Botton, S. Y. Savrasov, C. J. Humphreys, A. P. Sutton, *Phys. Rev. B* **1998**, 57, 1505.
- [5] H. Xu, D. Cheng, D. Cao, X. C. Zeng, *Nat. Catal.* **2018**, 1, 339.
- [6] V. V. Joost, H. Jürg, *J. Chem. Phys.* **2007**, 127, 4365.
- [7] J. Vandevondele, M. Krack, F. Mohamed, M. Parrinello, T. Chassaing, J. Hutter, *Comput. Phys. Commun.* **2005**, 167, 103.
- [8] S. Goedecker, M. Teter, J. Hutter, *Phys. Rev. B Condens. Matter.* **1995**, 54, 1703.
- [9] C. Hartwigsen, S. Goedecker, J. K. Hutter, *Phys. Rev. B* **1998**, 58, 3641.
- [10] J. Vandevondele, J. Hutter, *J. Chem. Phys.* **2007**, 127, 4365.
- [11] J. K. Nørskov, J. Rossmeisl, A. Logadottir, L. Lindqvist, J. R. Kitchin, T. Bligaard, H. J. K. Jonsson, *J. Phys. Chem. B* **2004**, 108, 17886.
- [12] H. Yang, Q. Lin, C. Zhang, X. Yu, Z. Cheng, G. Li, Q. Hu, X. Ren, Q. Zhang, J. Liu, *Nature Communications.* **2020**, 11, 593
- [13] T. Zheng, K. Jiang, N. Ta, Y. Hu, J. Zeng, J. Liu, H. Wang, *Joule* **2019**, 3, 265.
- [14] T. Möller, W. Ju, A. Bagger, X. Wang, F. Luo, T. Ngo Thanh, A. S. Varela, J. Rossmeisl, P. Strasser, *Energy Environ. Sci.* **2019**, 12, 640.
- [15] J. Gu, C.-S. Hsu, L. Bai, H. M. Chen, X. Hu, *Science* **2019**, 364, 1091.
- [16] H. B. Yang, S.-F. Hung, S. Liu, K. Yuan, S. Miao, L. Zhang, X. Huang, H.-Y. Wang, W. Cai, R. Chen, *Nature Energy* **2018**, 3, 140.
- [17] S. Ren, D. Joulié, D. Salvatore, K. Torbensen, M. Wang, M. Robert, C. P. Berlinguette, *Science*, 365, 367.
- [18] K. Jiang, S. Siahrostami, A. J. Akey, Y. Li, Z. Lu, J. Lattimer, Y. Hu, C. Stokes, M. Gangishetty, G. Chen, *Chem* **2017**, 3, 950.
- [19] E. Zhang, T. Wang, K. Yu, J. Liu, W. Chen, A. Li, H. Rong, R. Lin, S. Ji, X. Zheng, Y. Wang, L. Zheng, C. Chen, D. Wang, J. Zhang, Y. Li, *J. Am. Chem. Soc.* **2019**, 141, 16569.
- [20] Y. Cheng, S. Zhao, B. Johannessen, J. P. Veder, M. Saunders, M. R. Rowles, M. Cheng, C. Liu, M. F. Chisholm, M. R. De, *Adv. Mater.* **2018**, 30, 1706287.
- [21] F. Yang, P. Song, X. Liu, B. Mei, W. Xing, Z. Jiang, L. Gu, W. Xu, *Angew. Chem. Int. Ed.* **2018**, 57, 12303.
- [22] W. Zheng, F. Chen, Q. Zeng, Z. Li, B. Yang, L. Lei, Q. Zhang, F. He, X. Wu, Y. Hou, *Nano-Micro Letters* **2020**, 12, 108.
- [23] C. Zhao, X. Dai, T. Yao, W. Chen, X. Wang, J. Wang, J. Yang, S. Wei, Y. Wu, Y. Li, *J. Am. Chem. Soc.* **2017**, 139, 8078.

- [24] Jian, Yang, Zongyang, Qiu, Changming, Zhao, Weichen, Wei, Wenxing, Chen, *Angew. Chem. Int. Ed.* **2018**, 130, 14291.
- [25] K. Jiang, S. Siahrostami, T. Zheng, Y. Hu, S. Hwang, E. Stavitski, Y. Peng, J. J. Dynes, M. Gangishetty, D. Su, K. Attenkofer, H. Wang, *Energy Environ. Sci.* **2018**, 11, 893.
- [26] P. Lu, Y. Yang, J. Yao, M. Wang, S. Dipazir, M. Yuan, J. Zhang, X. Wang, Z. Xie, G. Zhang, *Appl. Catal. B-Environ.* **2019**, 241, 113.
- [27] W. Ju, A. Bagger, G. P. Hao, A. S. Varela, I. Sinev, V. Bon, C. B. Roldan, S. Kaskel, J. Rossmeisl, P. Strasser, *Nat. Commun.* **2017**, 8, 944.
- [28] F. Pan, H. Zhang, K. Liu, D. A. Cullen, K. L. More, M. Wang, Z. Feng, G. Wang, G. Wu, Y. Li, *ACS Catal.* **2018**, 4, 3116.
- [29] X. Wang, Z. Chen, X. Zhao, T. Yao, W. Chen, R. You, C. Zhao, G. Wu, J. Wang, W. Huang, *Angew. Chem. Int. Ed.* **2018**, 57, 1944.
- [30] Y. Ye, F. Cai, H. Li, H. Wu, G. Wang, Y. Li, S. Miao, S. Xie, R. Si, J. Wang, *Nano Energy* **2017**, 38, 281.
- [31] Y. Pan, R. Lin, Y. Chen, S. Liu, W. Zhu, X. Cao, W. Chen, K. Wu, W. C. Cheong, Y. Wang, L. Zheng, J. Luo, Y. Lin, Y. Liu, C. Liu, J. Li, Q. Lu, X. Chen, D. Wang, Q. Peng, C. Chen, Y. Li, *J. Am. Chem. Soc.* **2018**, 140, 4218.
- [32] X. Li, W. Bi, M. Chen, Y. Sun, H. Ju, W. Yan, J. Zhu, X. Wu, W. Chu, C. Wu, *J. Am. Chem. Soc.* **2017**, 139, 14889.
- [33] C. Zhao, Y. Wang, Z. Li, W. Chen, Q. Xu, D. He, D. Xi, Q. Zhang, T. Yuan, Y. Qu, J. Yang, F. Zhou, Z. Yang, X. Wang, J. Wang, J. Luo, Y. Li, H. Duan, Y. Wu, Y. Li, *Joule*, **2019**, 3, 584.
- [34] Y. Zhao, J. Liang, J. Ma, C. Wang, G. Wallace, *Adv. Energy Mater.* **2018**, 8, 1702524.
- [35] P. Hou, W. Song, X. Wang, Z. Hu, P. Kang, *Small* **2020**, 16, 2001896.
- [36] T. N. Huan, N. Ranjbar, G. Rousse, M. Sougrati, A. Zitolo, V. Mougel, F. Jaouen, M. Fontecave, *ACS Catal.* **2017**, 7, 1520.
- [37] Y. Cheng, S. Zhao, H. Li, S. He, J.-P. Veder, B. Johannessen, J. Xiao, S. Lu, J. Pan, M. F. Chisholm, S.-Z. Yang, C. Liu, J. G. Chen, S. P. Jiang, *Appl. Catal. B-Environ.* **2019**, 243, 294.
- [38] C. Zhang, S. Yang, J. Wu, M. Liu, S. Yazdi, M. Ren, J. Sha, J. Zhong, K. Nie, A. S. Jalilov, *Adv. Energy Mater.* **2018**, 8, 1703487.
- [39] J. Tuo, Y. Lin, Y. Zhu, H. Jiang, Y. Li, L. Cheng, R. Pang, J. Shen, L. Song, C. Li, *Appl. Catal. B-Environ.* **2020**, 272, 118960.